

A-PRIORI AND A-POSTERIORI ERROR ANALYSIS FOR THE FALK-TU FAMILY OF REISSNER-MINDLIN PLATE ELEMENTS

L. BEIRÃO DA VEIGA¹, C. CHINOSI², C. LOVADINA^{3,*} and R. STENBERG⁴

¹*Dipartimento di Matematica, Università degli Studi di Milano, Via Saldini 50
Milano I-20133, Italy. Email: Lourenco.Beirao@mat.unimi.it*

²*Dipartimento di Scienze e Tecnologie Avanzate, Università del Piemonte Orientale, Via
Bellini 25/G
Alessandria I-15100, Italy. Email: chinosi@mfn.unipmn.it*

³*Dipartimento di Matematica, Università di Pavia and IMATI-CNR, Via Ferrata 1
Pavia I-27100, Italy. Email: carlo.lovadina@unipv.it*

⁴*Institute of Mathematics, Helsinki University of Technology
P.O.Box 1100, 02015 TKK, Finland. Email: rolf.stenberg@hut.fi*

Abstract.

A family of plate elements introduced by Falk and Tu [25] is considered. A new stability and a-priori error analysis is given. In addition, an a-posteriori error estimate is proved. The analysis is confirmed by numerical benchmark computations.

AMS subject classification (2000): 65F20.

Key words: Reissner-Mindlin plates, finite element methods, a-priori error analysis, a-posteriori error analysis.

1 Introduction

The finite element simulation of Reissner-Mindlin plates has been an active research area, due both to its practical importance, and to the non-trivial problems to overcome. In particular, non-standard techniques need to be used to avoid the shear-locking phenomenon, as well as the occurrence of spurious modes and boundary layer effects. By now, the roots of the above-mentioned troubles are well-understood, and several strategies have been proposed and analyzed. However, most of the mathematical literature on the subject is addressed to establish a-priori error estimates for the schemes under consideration, cf. [1], [12], [14], [24], [27], [32], [36], and the references therein. On the contrary, for the a-posteriori error analysis of plates, only relatively few results are available. To the our best knowledge, most of the relevant mathematical literature is restricted to the works [15]–[17], [26], [29], and [7]–[9].

In this paper we present an analysis of the Reissner-Mindlin plate elements proposed and studied by Falk and Tu [25]. We first give an alternative a-priori error analysis (see Section 3). In particular, we provide a stability result

*Corresponding author.

which will be the basis of the a-posteriori error estimates obtained in Section 4. Moreover, we prove a new convergence result, confirming the locking-free features of the elements under consideration. In the a-posteriori analysis we establish the equivalence, uniformly in the plate thickness, between a suitable residual-based estimator and the error, measured by means of the norm introduced in Section 3. To obtain such a result, we use the technique of [29]. We notice that we make use of a *saturation assumption* to prove the reliability of our estimator (cf. Section 4.2. Finally, we present a set of numerical experiments, which show the actual performances of the lowest order element in the Falk-Tu family, along with its corresponding error estimator. Our numerical tests confirm the theoretical predictions concerning both the a-priori and the a-posteriori analysis.

Throughout the paper we will use standard notations for Sobolev norms and seminorms. Moreover, we will denote with C a generic constant which may take different values in different occurrences, and which is independent of the mesh parameter h and the plate thickness t .

2 The Reissner-Mindlin problem and the finite element discretization

The Reissner-Mindlin problem, for a plate with polygonal mid-plane Ω , is to find $(\boldsymbol{\theta}, w, \boldsymbol{\gamma})$ such that

$$(2.1) \quad \left\{ \begin{array}{ll} -\operatorname{div} \mathbf{C}\boldsymbol{\varepsilon}(\boldsymbol{\theta}) - \boldsymbol{\gamma} = \mathbf{0} & \text{in } \Omega, \\ -\operatorname{div} \boldsymbol{\gamma} = g & \text{in } \Omega, \\ \boldsymbol{\gamma} = \mu t^{-2}(\nabla w - \boldsymbol{\theta}) & \text{in } \Omega, \\ \boldsymbol{\theta} = \mathbf{0}, w = 0 & \text{on } \Gamma_C, \\ \boldsymbol{\theta} \cdot \mathbf{t} = 0, w = 0, (\mathbf{C}\boldsymbol{\varepsilon}(\boldsymbol{\theta})\mathbf{n}) \cdot \mathbf{n} = 0 & \text{on } \Gamma_H, \\ w = 0, \mathbf{C}\boldsymbol{\varepsilon}(\boldsymbol{\theta})\mathbf{n} = 0 & \text{on } \Gamma_S, \\ \mathbf{C}\boldsymbol{\varepsilon}(\boldsymbol{\theta})\mathbf{n} = \mathbf{0}, \boldsymbol{\gamma} \cdot \mathbf{n} = 0 & \text{on } \Gamma_F. \end{array} \right.$$

Here, the boundary $\partial\Omega$ is split into four non-overlapping parts Γ_C , Γ_H , Γ_S and Γ_F , where clamped, hard simply supported, soft simply supported and free boundary conditions are imposed. We assume that Γ_C has positive measure. Moreover, \mathbf{C} is the tensor of bending moduli, $\boldsymbol{\theta}$ represents the rotations, w the transversal displacement, $\boldsymbol{\gamma}$ the scaled shear force and g a given transversal load. Finally, $\boldsymbol{\varepsilon}$ is the usual symmetric gradient operator, μ is the shear modulus, and t is the thickness. The variational formulation of problem (2.1) is:

$$(2.2) \quad \left\{ \begin{array}{ll} \text{Find } (\boldsymbol{\theta}, w, \boldsymbol{\gamma}) \in \boldsymbol{\Theta} \times W \times \boldsymbol{\Gamma} \text{ such that} & \\ a(\boldsymbol{\theta}, \boldsymbol{\eta}) + (\nabla w - \boldsymbol{\eta}, \boldsymbol{\gamma}) = (g, v) & \forall (\boldsymbol{\eta}, v) \in \boldsymbol{\Theta} \times W, \\ (\nabla w - \boldsymbol{\theta}, \boldsymbol{\tau}) - \mu^{-1}t^2(\boldsymbol{\gamma}, \boldsymbol{\tau}) = 0 & \forall \boldsymbol{\tau} \in [L^2(\Omega)]^2, \end{array} \right.$$

where

$$(2.3) \quad \begin{aligned} \Theta &= \{ \boldsymbol{\eta} \in [H^1(\Omega)]^2 \mid \boldsymbol{\eta} = \mathbf{0} \text{ on } \Gamma_C ; \boldsymbol{\eta} \cdot \mathbf{t} = 0 \text{ on } \Gamma_H \}, \\ W &= \{ v \in H^1(\Omega) \mid v = 0 \text{ on } \Gamma_C \cup \Gamma_S \} \end{aligned}$$

and (\cdot, \cdot) denotes the inner-product in $L^2(\Omega)$ and $[L^2(\Omega)]^2$. The bilinear form $a(\cdot, \cdot)$ is defined by

$$a(\boldsymbol{\theta}, \boldsymbol{\eta}) := \int_{\Omega} \mathbf{C} \boldsymbol{\varepsilon}(\boldsymbol{\theta}) : \boldsymbol{\varepsilon}(\boldsymbol{\eta}).$$

Following [18], we write the pair $(\boldsymbol{\theta}, w)$ as

$$(2.4) \quad (\boldsymbol{\theta}, w) = (\boldsymbol{\theta}_0 + \boldsymbol{\theta}_r, w_0 + w_r),$$

where $(\boldsymbol{\theta}_0, w_0)$ is the solution of the Kirchhoff-type limit problem:

$$(2.5) \quad \begin{cases} \text{Find } (\boldsymbol{\theta}_0, w_0, \boldsymbol{\gamma}_0) \in \Theta \times W \times \Gamma \text{ such that} \\ a(\boldsymbol{\theta}_0, \boldsymbol{\eta}) + \langle \nabla v - \boldsymbol{\eta}, \boldsymbol{\gamma}_0 \rangle = (g, v) & \forall (\boldsymbol{\eta}, v) \in \Theta \times W, \\ \langle \nabla w_0 - \boldsymbol{\theta}_0, \boldsymbol{\tau} \rangle = 0 & \forall \boldsymbol{\tau} \in \Gamma, \end{cases}$$

and $(\boldsymbol{\theta}_r, w_r)$ can be thought as a remainder. Here, $\langle \cdot, \cdot \rangle$ is the duality pairing between $\mathbf{H}_{0, \Gamma_D}(\text{rot}, \Omega) = \{ \boldsymbol{\tau} \in \mathbf{H}(\text{rot}, \Omega) \mid \boldsymbol{\tau} \cdot \mathbf{t} = 0 \text{ on } \Gamma_C \cup \Gamma_H \}$ and its dual $\Gamma = (\mathbf{H}_{0, \Gamma_D}(\text{rot}, \Omega))'$. For the clamped plate, i.e. $\Gamma_C = \partial\Omega$, one has the following result (cf. [31]).

PROPOSITION 2.1. *Let Ω be a convex polygonal domain and let Ω_i be a domain compactly embedded in Ω . Denote by $(w, \boldsymbol{\theta}, \boldsymbol{\gamma})$ the Reissner–Mindlin solution for the clamped plate and let $w = w_0 + w_r$, where w_0 is the deflection obtained from the limit problem (2.5). With $g \in H^{s-2}(\Omega)$ and $tg \in H^{s-1}(\Omega)$, $s \geq 1$, it then holds*

$$(2.6) \quad \|w_0\|_2 + t^{-1}\|w_r\|_1 + \|\boldsymbol{\theta}\|_1 + \|\boldsymbol{\gamma}\|_{-1} + t\|\boldsymbol{\gamma}\|_0 \leq C(\|g\|_{-2} + t\|g\|_{-1}),$$

$$(2.7) \quad \|w_0\|_3 + t^{-1}\|w_r\|_2 + \|\boldsymbol{\theta}\|_2 + \|\boldsymbol{\gamma}\|_0 + t\|\boldsymbol{\gamma}\|_1 \leq C(\|g\|_{-1} + t\|g\|_0)$$

and

$$(2.8) \quad \begin{aligned} \|w_0\|_{s+2, \Omega_i} + t^{-1}\|w_r\|_{s+1, \Omega_i} + \|\boldsymbol{\theta}\|_{s+1, \Omega_i} + \|\boldsymbol{\gamma}\|_{s-1, \Omega_i} + t\|\boldsymbol{\gamma}\|_{s, \Omega_i} \\ \leq C(\|g\|_{s-2} + t\|g\|_{s-1}). \end{aligned}$$

□

Let \mathcal{T}_h be a sequence of decompositions of Ω into triangular elements T , satisfying the usual compatibility conditions (see [22]). We also assume that the family \mathcal{T}_h is regular, i.e. there exists a constant $\sigma > 0$ such that

$$(2.9) \quad h_T \leq \sigma \rho_T \quad \forall T \in \mathcal{T}_h,$$

where h_T is the diameter of the element T and ρ_T is the maximum diameter of the circles contained in T . Moreover, given the decomposition \mathcal{T}_h we will denote with \mathcal{E}_h the set of all the edges E of the triangles $T \in \mathcal{T}_h$, and with $\mathcal{E}_h^I \subset \mathcal{E}_h$ the set of all internal edges. The subset of boundary edges will instead be indicated with \mathcal{E}_h^C , \mathcal{E}_h^H , \mathcal{E}_h^S and \mathcal{E}_h^F , representing respectively the set of edges laying in Γ_C , Γ_H , Γ_S and Γ_F .

The family to be considered uses the FE spaces (see [25]), for $k \geq 1$:

$$(2.10) \quad \Theta_h = \{ \boldsymbol{\eta} \in \Theta \mid \boldsymbol{\eta}|_T \in [P_k(T) + B_{k+3}(T)]^2 \ \forall T \in \mathcal{T}_h \},$$

$$(2.11) \quad W_h = \{ v \in W \mid v|_T \in P_{k+1}(T) \ \forall T \in \mathcal{T}_h \},$$

$$(2.12) \quad \Gamma_h = \{ \boldsymbol{\tau} \in [L^2(\Omega)]^2 \mid \boldsymbol{\tau}|_T \in [P_k(T)]^2 \ \forall T \in \mathcal{T}_h \},$$

where $P_l(T)$, $l = k, k+1$, is the space of polynomials of degree l defined on T , and $B_{k+3}(T) = P_{k+3}(T) \cap H_0^1(T)$ is a space of bubbles on T . Then, we consider the discrete problem:

$$(2.13) \quad \begin{cases} \text{Find } (\boldsymbol{\theta}_h, w_h; \boldsymbol{\gamma}_h) \in \Theta_h \times W_h \times \Gamma_h \text{ such that} \\ a(\boldsymbol{\theta}_h, \boldsymbol{\eta}) + (\boldsymbol{\gamma}_h, \nabla v - \boldsymbol{\eta}) = (g, v) & \forall (\boldsymbol{\eta}, v) \in \Theta_h \times W_h, \\ (\nabla w_h - \boldsymbol{\theta}_h, \boldsymbol{\tau}) - \mu^{-1} t^2 (\boldsymbol{\gamma}_h, \boldsymbol{\tau}) = 0 & \forall \boldsymbol{\tau} \in \Gamma_h. \end{cases}$$

REMARK 2.1. *We point out that eliminating $\boldsymbol{\gamma}_h$ from system (2.13), our scheme is equivalent to the following problem involving only the rotations and the vertical displacements:*

$$(2.14) \quad \begin{cases} \text{Find } (\boldsymbol{\theta}_h, w_h) \in \Theta_h \times W_h \text{ such that} \\ a(\boldsymbol{\theta}_h, \boldsymbol{\eta}) + \mu t^{-2} (\nabla w_h - \mathbf{\Pi}_h \boldsymbol{\theta}_h, \nabla v - \mathbf{\Pi}_h \boldsymbol{\eta}) = (g, v) & \forall (\boldsymbol{\eta}, v) \in \Theta_h \times W_h, \end{cases}$$

where $\mathbf{\Pi}_h$ denotes the L^2 -projection operator onto Γ_h . We note that in obtaining (2.14) we need to use the fundamental property (cf. (2.11) and (2.12))

$$(2.15) \quad \nabla W_h \subset \Gamma_h.$$

3 The stability and a-priori error analysis

By denoting

$$(3.1) \quad \begin{aligned} \mathcal{B}(\boldsymbol{\theta}, w, \boldsymbol{\gamma}; \boldsymbol{\eta}, v, \boldsymbol{\tau}) := & a(\boldsymbol{\theta}, \boldsymbol{\eta}) + (\nabla v - \boldsymbol{\eta}, \boldsymbol{\gamma}) \\ & + (\nabla w - \boldsymbol{\theta}, \boldsymbol{\tau}) - \mu^{-1} t^2 (\boldsymbol{\gamma}, \boldsymbol{\tau}), \end{aligned}$$

the continuous problem (2.2) reads

$$(3.2) \quad \begin{cases} \text{Find } (\boldsymbol{\theta}, w; \boldsymbol{\gamma}) \in \Theta \times W \times [L^2(\Omega)]^2 \text{ such that} \\ \mathcal{B}(\boldsymbol{\theta}, w, \boldsymbol{\gamma}; \boldsymbol{\eta}, v, \boldsymbol{\tau}) = (g, v) & \forall (\boldsymbol{\eta}, v; \boldsymbol{\tau}) \in \Theta \times W \times [L^2(\Omega)]^2, \end{cases}$$

while the discrete problem (2.13) is

$$(3.3) \quad \begin{cases} \text{Find } (\boldsymbol{\theta}_h, w_h; \boldsymbol{\gamma}_h) \in \boldsymbol{\Theta}_h \times W_h \times \boldsymbol{\Gamma}_h \text{ such that} \\ \mathcal{B}(\boldsymbol{\theta}_h, w_h, \boldsymbol{\gamma}_h; \boldsymbol{\eta}, v, \boldsymbol{\tau}) = (g, v) \quad \forall (\boldsymbol{\eta}, v; \boldsymbol{\tau}) \in \boldsymbol{\Theta}_h \times W_h \times \boldsymbol{\Gamma}_h. \end{cases}$$

Following the lines of [18, 28, 29, 32, 36], we prove a priori error estimates with respect to the norms

$$(3.4) \quad |||(\boldsymbol{\eta}, v)|||_h^2 := \|\boldsymbol{\eta}\|_1^2 + \|v\|_1^2 + \sum_{T \in \mathcal{T}_h} \frac{1}{h_T^2 + t^2} \|\nabla v - \boldsymbol{\eta}\|_{0,T}^2 \quad \forall (\boldsymbol{\eta}, v) \in \boldsymbol{\Theta} \times W$$

and

$$(3.5) \quad \|\boldsymbol{\tau}\|_{\boldsymbol{\Theta}'} + t\|\boldsymbol{\tau}\|_0 \quad \forall \boldsymbol{\tau} \in [L^2(\Omega)]^2.$$

Above, $\|\cdot\|_{\boldsymbol{\Theta}'}$ denotes the norm in $\boldsymbol{\Theta}'$, the dual space of $\boldsymbol{\Theta}$.

REMARK 3.1. *For a clamped plate, we have $\boldsymbol{\Theta} = [H_0^1(\Omega)]^2$. Therefore, the norm $\|\cdot\|_{\boldsymbol{\Theta}'}$ is the usual norm in $[H^{-1}(\Omega)]^2$.*

We will also use the following discrete norm

$$(3.6) \quad \|\boldsymbol{\tau}\|_h^2 := \sum_{T \in \mathcal{T}_h} h_T^2 \|\boldsymbol{\tau}\|_{0,T}^2 + t^2 \|\boldsymbol{\tau}\|_0^2 \quad \forall \boldsymbol{\tau} \in [L^2(\Omega)]^2.$$

Before proceeding, we need the following lemma, which establishes a suitable norm equivalence in the used finite element spaces.

LEMMA 3.1. *For each $(\boldsymbol{\eta}, v) \in \boldsymbol{\Theta}_h \times W_h$ it holds*

$$(3.7) \quad \left(\|\boldsymbol{\eta}\|_1^2 + \sum_{T \in \mathcal{T}_h} \frac{1}{h_T^2 + t^2} \|\nabla v - \boldsymbol{\Pi}_h \boldsymbol{\eta}\|_{0,T}^2 \right)^{1/2} \leq |||(\boldsymbol{\eta}, v)|||_h$$

and

$$(3.8) \quad |||(\boldsymbol{\eta}, v)|||_h \leq C \left(\|\boldsymbol{\eta}\|_1^2 + \sum_{T \in \mathcal{T}_h} \frac{1}{h_T^2 + t^2} \|\nabla v - \boldsymbol{\Pi}_h \boldsymbol{\eta}\|_{0,T}^2 \right)^{1/2}.$$

PROOF. Since (3.7) is trivial, we only consider (3.8). Therefore, take $\boldsymbol{\eta} \in \boldsymbol{\Theta}_h$, and $v \in W_h$. We write

$$(3.9) \quad \nabla v - \boldsymbol{\eta} = (\nabla v - \boldsymbol{\Pi}_h \boldsymbol{\eta}) + (\boldsymbol{\Pi}_h \boldsymbol{\eta} - \boldsymbol{\eta}),$$

so that we get

$$(3.10) \quad \begin{aligned} \|\nabla v - \boldsymbol{\eta}\|_{0,T}^2 &\leq 2 \left(\|\nabla v - \boldsymbol{\Pi}_h \boldsymbol{\eta}\|_{0,T}^2 + \|\boldsymbol{\Pi}_h \boldsymbol{\eta} - \boldsymbol{\eta}\|_{0,T}^2 \right) \\ &\leq C \left(\|\nabla v - \boldsymbol{\Pi}_h \boldsymbol{\eta}\|_{0,T}^2 + h_T^2 \|\boldsymbol{\eta}\|_{1,T}^2 \right) \end{aligned}$$

Therefore, we obtain

$$(3.11) \quad \begin{aligned} \frac{1}{h_T^2 + t^2} \|\nabla v - \boldsymbol{\eta}\|_{0,T}^2 &\leq C \left(\frac{1}{h_T^2 + t^2} \|\nabla v - \mathbf{\Pi}_h \boldsymbol{\eta}\|_{0,T}^2 + \frac{h_T^2}{h_T^2 + t^2} |\boldsymbol{\eta}|_{1,T}^2 \right) \\ &\leq C \left(\frac{1}{h_T^2 + t^2} \|\nabla v - \mathbf{\Pi}_h \boldsymbol{\eta}\|_{0,T}^2 + |\boldsymbol{\eta}|_{1,T}^2 \right). \end{aligned}$$

Summing over all the triangle contributions, we get

$$(3.12) \quad \sum_{T \in \mathcal{T}_h} \frac{1}{h_T^2 + t^2} \|\nabla v - \boldsymbol{\eta}\|_{0,T}^2 \leq C \left(\sum_{T \in \mathcal{T}_h} \frac{1}{h_T^2 + t^2} \|\nabla v - \mathbf{\Pi}_h \boldsymbol{\eta}\|_{0,T}^2 + \|\boldsymbol{\eta}\|_1^2 \right).$$

Furthermore, Poincaré's inequality yields

$$(3.13) \quad \begin{aligned} \|v\|_1 &\leq C \|\nabla v\|_0 \leq C (\|\nabla v - \boldsymbol{\eta}\|_0 + \|\boldsymbol{\eta}\|_0) \\ &\leq C \left[\left(\sum_{T \in \mathcal{T}_h} \frac{1}{h_T^2 + t^2} \|\nabla v - \boldsymbol{\eta}\|_{0,T}^2 \right)^{1/2} + \|\boldsymbol{\eta}\|_1 \right]. \end{aligned}$$

The estimate (3.8) now follows from (3.12)–(3.13). \square

By known techniques (cf. [18, 28, 32, 36]) we prove the following stability result.

PROPOSITION 3.2. *Given $(\boldsymbol{\beta}, z; \boldsymbol{\rho}) \in \boldsymbol{\Theta}_h \times W_h \times \boldsymbol{\Gamma}_h$ there exists $(\boldsymbol{\eta}, v; \boldsymbol{\tau}) \in \boldsymbol{\Theta}_h \times W_h \times \boldsymbol{\Gamma}_h$ such that*

$$(3.14) \quad \mathcal{B}(\boldsymbol{\beta}, z, \boldsymbol{\rho}; \boldsymbol{\eta}, v, \boldsymbol{\tau}) \geq C \left(\|(\boldsymbol{\beta}, z)\|_h^2 + \|\boldsymbol{\rho}\|_h^2 \right),$$

and

$$(3.15) \quad \|(\boldsymbol{\eta}, v)\|_h + \|\boldsymbol{\tau}\|_h \leq C \left(\|(\boldsymbol{\beta}, z)\|_h + \|\boldsymbol{\rho}\|_h \right)$$

PROOF. Let $(\boldsymbol{\beta}, z; \boldsymbol{\rho})$ be given in $\boldsymbol{\Theta}_h \times W_h \times \boldsymbol{\Gamma}_h$. Using exactly the same arguments of [18] and [28] we get that there exists $(\boldsymbol{\eta}, v; \boldsymbol{\tau})$ in $\boldsymbol{\Theta}_h \times W_h \times \boldsymbol{\Gamma}_h$ such that

$$(3.16) \quad \mathcal{B}(\boldsymbol{\beta}, z, \boldsymbol{\rho}; \boldsymbol{\eta}, v, \boldsymbol{\tau}) \geq C \left(\|\boldsymbol{\beta}\|_1^2 + \sum_{T \in \mathcal{T}_h} \frac{1}{h_T^2 + t^2} \|\nabla z - \mathbf{\Pi}_h \boldsymbol{\beta}\|_{0,T}^2 + \|\boldsymbol{\rho}\|_h^2 \right)$$

and

$$(3.17) \quad \begin{aligned} \|\boldsymbol{\eta}\|_1 + \left(\sum_{T \in \mathcal{T}_h} \frac{1}{h_T^2 + t^2} \|\nabla v - \mathbf{\Pi}_h \boldsymbol{\eta}\|_{0,T}^2 \right)^{1/2} + \|\boldsymbol{\tau}\|_h \\ \leq C \left(\|\boldsymbol{\beta}\|_1 + \left(\sum_{T \in \mathcal{T}_h} \frac{1}{h_T^2 + t^2} \|\nabla z - \mathbf{\Pi}_h \boldsymbol{\beta}\|_{0,T}^2 \right)^{1/2} + \|\boldsymbol{\rho}\|_h \right). \end{aligned}$$

The assertion now follows from the equivalence of norms given in Lemma 3.1. \square

It is now easy to prove the following result.

THEOREM 3.3. *It holds*

$$(3.18) \quad \begin{aligned} & \|\|(\boldsymbol{\theta} - \boldsymbol{\theta}_h, w - w_h)\|\|_h + \|\gamma - \gamma_h\|_h + \|\gamma - \gamma_h\|_{\boldsymbol{\Theta}'} \\ & \leq C \inf_{(\boldsymbol{\eta}, v, \boldsymbol{\tau}) \in \boldsymbol{\Theta}_h \times W_h \times \boldsymbol{\Gamma}_h} \{\|\|(\boldsymbol{\theta} - \boldsymbol{\eta}, w - v)\|\|_h + \|\gamma - \boldsymbol{\tau}\|_h\}. \end{aligned}$$

PROOF. By noting that our method is consistent (see (3.2) and (3.3)), and by Proposition 3.2, a standard “consistency–stability argument” immediately gives the estimate

$$(3.19) \quad \begin{aligned} & \|\|(\boldsymbol{\theta} - \boldsymbol{\theta}_h, w - w_h)\|\|_h + \|\gamma - \gamma_h\|_h \\ & \leq C \inf_{(\boldsymbol{\eta}, v, \boldsymbol{\tau}) \in \boldsymbol{\Theta}_h \times W_h \times \boldsymbol{\Gamma}_h} \{\|\|(\boldsymbol{\theta} - \boldsymbol{\eta}, w - v)\|\|_h + \|\gamma - \boldsymbol{\tau}\|_h\}. \end{aligned}$$

To get the shear error in the norm of $\boldsymbol{\Theta}'$, an application of the “Pitkäranta-Verfürth trick” (cf. [34, 39] and [29]) leads to

$$(3.20) \quad \|\gamma - \gamma_h\|_{\boldsymbol{\Theta}'} \leq C (\|\gamma - \gamma_h\|_h + \|\boldsymbol{\theta} - \boldsymbol{\theta}_h\|_1).$$

Estimates (3.19) and (3.20) imply the bound (3.18). \square

For the special case of clamped plate and a convex domain the techniques of [32] gives the the following estimate.

PROPOSITION 3.4. *Let Ω be a convex polygon and let Ω_i be a domain compactly embedded in Ω . For $g \in H^{k-2}(\Omega)$, $tg \in H^{k-1}(\Omega)$ it holds*

$$(3.21) \quad \begin{aligned} & \|\|(\boldsymbol{\theta} - \boldsymbol{\theta}_h, w - w_h)\|\|_h + t\|\gamma - \gamma_h\|_0 + \|\gamma - \gamma_h\|_{-1} \\ & \leq C \{h_i^k (\|g\|_{k-2} + t\|g\|_{k-1}) + h_b (\|g\|_{-1} + t\|g\|_0)\}, \end{aligned}$$

$$(3.22) \quad \|\boldsymbol{\theta} - \boldsymbol{\theta}_h\|_0 \leq Ch \{h_i^k (\|g\|_{k-2} + t\|g\|_{k-1}) + h_b (\|g\|_{-1} + t\|g\|_0)\}$$

and

$$(3.23) \quad \|w - w_h\|_1 \leq C(h + t) \{h_i^k (\|g\|_{k-2} + t\|g\|_{k-1}) + h_b (\|g\|_{-1} + t\|g\|_0)\},$$

where

$$(3.24) \quad h_i := \max_{T \subset \Omega_i} h_T \quad ; \quad h_b := \max_{T \not\subset \Omega_i} h_T.$$

4 A posteriori error estimates

In this section we introduce the error estimator and we study its reliability and efficiency. The edge set \mathcal{E}_h we split into

$$(4.1) \quad \mathcal{E}_h = \mathcal{E}_h^I \cup \mathcal{E}_h^F \cup \mathcal{E}_h^S \cup \mathcal{E}_h^H,$$

where \mathcal{E}_h^I is the set of the inner edges, while \mathcal{E}_h^F , \mathcal{E}_h^S and \mathcal{E}_h^H are the sets where free, soft simply supported and hard simply supported boundary conditions are imposed. For each $T \in \mathcal{T}_h$ we introduce the following quantity

$$(4.2) \quad \begin{aligned} \tilde{\eta}_T^2 := & h_T^2 \|\mathbf{div} \mathbf{C}\varepsilon(\boldsymbol{\theta}_h) + \boldsymbol{\gamma}_h\|_{0,T}^2 + h_T^2 (h_T^2 + t^2) \|\mathbf{div} \boldsymbol{\gamma}_h + g_h\|_{0,T}^2 \\ & + \frac{\mu^2}{h_T^2 + t^2} \|\mu^{-1} t^2 \boldsymbol{\gamma}_h - (\nabla w_h - \boldsymbol{\theta}_h)\|_{0,T}^2, \end{aligned}$$

where g_h is an approximation of the load g . Moreover, we set

$$(4.3) \quad \begin{aligned} \eta_E^2 := & h_E \|\llbracket \mathbf{C}\varepsilon(\boldsymbol{\theta}_h) \mathbf{n} \rrbracket\|_{0,E}^2 + h_E (h_E^2 + t^2) \|\llbracket \boldsymbol{\gamma}_h \cdot \mathbf{n} \rrbracket\|_{0,E}^2 & E \in \mathcal{E}_h^I \cup \mathcal{E}_h^F, \\ \eta_S^2 := & h_E \|\llbracket \mathbf{C}\varepsilon(\boldsymbol{\theta}_h) \mathbf{n} \rrbracket\|_{0,E}^2 & E \in \mathcal{E}_h^S, \\ \eta_H^2 := & h_E \|(\llbracket \mathbf{C}\varepsilon(\boldsymbol{\theta}_h) \mathbf{n} \rrbracket) \cdot \mathbf{n}\|_{0,E}^2 & E \in \mathcal{E}_h^H, \end{aligned}$$

where h_E is the length of the side E and $\llbracket \cdot \rrbracket$ denotes the jump operator. We adopt the usual notation that the jump operator on a boundary edge is equal to the restriction operator on that edge. We then define the local indicator η_T as

$$(4.4) \quad \eta_T := \left(\tilde{\eta}_T^2 + \sum_{E \subset \partial T \cap (\mathcal{E}_h^I \cup \mathcal{E}_h^F)} \eta_E^2 + \sum_{E \subset \partial T \cap \mathcal{E}_h^S} \eta_S^2 + \sum_{E \subset \partial T \cap \mathcal{E}_h^H} \eta_H^2 \right)^{1/2},$$

and the global indicator η as

$$(4.5) \quad \eta := \left(\sum_{T \in \mathcal{T}_h} \tilde{\eta}_T^2 + \sum_{E \in \mathcal{E}_h^I \cup \mathcal{E}_h^F} \eta_E^2 + \sum_{E \in \mathcal{E}_h^S} \eta_S^2 + \sum_{E \in \mathcal{E}_h^H} \eta_H^2 \right)^{1/2}.$$

4.1 Lower bounds

The efficiency of the error estimator we prove using the techniques of [29].

PROPOSITION 4.1. *Let $(\boldsymbol{\theta}, w; \boldsymbol{\gamma})$ (resp. $(\boldsymbol{\theta}_h, w_h; \boldsymbol{\gamma}_h)$) be the solution of the continuous (respectively discrete) problem. Given $T \in \mathcal{T}_h$, it holds*

$$(4.6) \quad \begin{aligned} \eta_T \leq & C \left(\frac{1}{(h_T^2 + t^2)^{1/2}} \|\nabla(w_h - w) - (\boldsymbol{\theta}_h - \boldsymbol{\theta})\|_{0,T} + \|\boldsymbol{\theta}_h - \boldsymbol{\theta}\|_{1,\omega_T} \right. \\ & + \|\boldsymbol{\gamma}_h - \boldsymbol{\gamma}\|_{\boldsymbol{\Theta}(\omega_T)'} + t \|\boldsymbol{\gamma}_h - \boldsymbol{\gamma}\|_{0,\omega_T} \\ & \left. + \left(\sum_{T' \subset \omega_T} h_{T'}^2 (h_{T'}^2 + t^2) \|g - g_h\|_{0,T'}^2 \right)^{1/2} \right), \end{aligned}$$

where η_T is defined by (4.2)–(4.4), and ω_T is the union of the triangles in \mathcal{T}_h sharing a side with T . Moreover, $\boldsymbol{\Theta}(\omega_T)'$ is the dual of the space

$$\boldsymbol{\Theta}(\omega_T) = \{\boldsymbol{\eta}|_{\omega_T} \mid \boldsymbol{\eta} \in \boldsymbol{\Theta} \text{ and } \boldsymbol{\eta} = \mathbf{0} \text{ on } \partial\omega_T \setminus \partial\Omega\}.$$

PROOF. We fix a triangle $T \in \mathcal{T}_h$. Arguing as in [29], we can obtain

$$\begin{aligned}
& \left(\tilde{\eta}_T^2 + \sum_{E \subset \partial T \cap \mathcal{E}_h^i} \eta_E^2 \right)^{1/2} \\
(4.7) \quad & \leq C \left(\frac{1}{(h_T^2 + t^2)^{1/2}} \|\nabla(w_h - w) - (\boldsymbol{\theta}_h - \boldsymbol{\theta})\|_{0,T} + \|\boldsymbol{\theta}_h - \boldsymbol{\theta}\|_{1,\omega_T} \right. \\
& \quad + \|\boldsymbol{\gamma}_h - \boldsymbol{\gamma}\|_{-1,\omega_T} + t \|\boldsymbol{\gamma}_h - \boldsymbol{\gamma}\|_{0,\omega_T} \\
& \quad \left. + \left(\sum_{T' \subset \omega_T} h_{T'}^2 (h_{T'}^2 + t^2) \|g - g_h\|_{0,T'}^2 \right)^{1/2} \right).
\end{aligned}$$

If the triangle T contains a boundary edge $E \in \mathcal{E}_h^F$, the same technique leads to the estimate

$$\begin{aligned}
(4.8) \quad \eta_E & \leq C \left(\|\boldsymbol{\theta}_h - \boldsymbol{\theta}\|_{1,T} + \|\boldsymbol{\gamma}_h - \boldsymbol{\gamma}\|_{\boldsymbol{\Theta}(T)'} + t \|\boldsymbol{\gamma}_h - \boldsymbol{\gamma}\|_{0,T} \right. \\
& \quad \left. + h_T (h_T + t) \|g - g_h\|_{0,T} \right),
\end{aligned}$$

where $\boldsymbol{\Theta}(T)'$ is the dual space of

$$\boldsymbol{\Theta}(T) = \{\boldsymbol{\eta}|_T \mid \boldsymbol{\eta} \in \boldsymbol{\Theta} \text{ and } \boldsymbol{\eta} = \mathbf{0} \text{ on } \partial T \setminus \partial\Omega\}.$$

Similarly, for boundary edges $E \in \mathcal{E}_h^S$ and $E \in \mathcal{E}_h^H$, we respectively get

$$(4.9) \quad \eta_S \leq C \left(\|\boldsymbol{\theta}_h - \boldsymbol{\theta}\|_{1,T} + \|\boldsymbol{\gamma}_h - \boldsymbol{\gamma}\|_{\boldsymbol{\Theta}(T)'} + t \|\boldsymbol{\gamma}_h - \boldsymbol{\gamma}\|_{0,T} \right),$$

and

$$(4.10) \quad \eta_H \leq C \left(\|\boldsymbol{\theta}_h - \boldsymbol{\theta}\|_{1,T} + \|\boldsymbol{\gamma}_h - \boldsymbol{\gamma}\|_{\boldsymbol{\Theta}(T)'} + t \|\boldsymbol{\gamma}_h - \boldsymbol{\gamma}\|_{0,T} \right).$$

Since it holds

$$\begin{aligned}
(4.11) \quad & \|\boldsymbol{\gamma}_h - \boldsymbol{\gamma}\|_{-1,\omega_T} \leq \|\boldsymbol{\gamma}_h - \boldsymbol{\gamma}\|_{\boldsymbol{\Theta}(\omega_T)'} \\
& \|\boldsymbol{\gamma}_h - \boldsymbol{\gamma}\|_{\boldsymbol{\Theta}(T)'} \leq \|\boldsymbol{\gamma}_h - \boldsymbol{\gamma}\|_{\boldsymbol{\Theta}(\omega_T)'},
\end{aligned}$$

(4.6) follows from (4.7)–(4.10). \square

4.2 Upper bounds

We now prove the reliability of the error estimator. Given an integer $k \geq 1$ (and, therefore, an element in the Falk-Tu family), we will prove our upper bounds by means of a saturation assumption involving the higher order $(k+1)$ -th Falk-Tu element. In order to avoid cumbersome notation, we will denote all the quantities relative to this latter element by a "tilde". We will use the following

Saturation assumption: Let $(\boldsymbol{\theta}_h, w_h, \boldsymbol{\gamma}_h) \in \boldsymbol{\Theta}_h \times W_h \times \boldsymbol{\Gamma}_h$ and $(\tilde{\boldsymbol{\theta}}_h, \tilde{w}_h, \tilde{\boldsymbol{\gamma}}_h) \in \tilde{\boldsymbol{\Theta}}_h \times W_h \times \tilde{\boldsymbol{\Gamma}}_h$ be the discrete solutions using the k -th and $(k+1)$ -th Falk-Tu element, respectively. We assume that there exists $0 < \rho < 1$ such that

$$(4.12) \quad \begin{aligned} & |||(\boldsymbol{\theta} - \tilde{\boldsymbol{\theta}}_h, w - \tilde{w}_h)|||_h + \|\boldsymbol{\gamma} - \tilde{\boldsymbol{\gamma}}_h\|_{\boldsymbol{\Theta}'} + t \|\boldsymbol{\gamma} - \tilde{\boldsymbol{\gamma}}_h\|_0 \\ & \leq \rho \left(|||(\boldsymbol{\theta} - \boldsymbol{\theta}_h, w - w_h)|||_h + \|\boldsymbol{\gamma} - \boldsymbol{\gamma}_h\|_{\boldsymbol{\Theta}'} + t \|\boldsymbol{\gamma} - \boldsymbol{\gamma}_h\|_0 \right). \end{aligned}$$

□

By using the saturation assumption (4.12), it is easily seen that one gets the reliability estimate

$$(4.13) \quad \begin{aligned} & |||(\boldsymbol{\theta} - \boldsymbol{\theta}_h, w - w_h)|||_h + \|\boldsymbol{\gamma} - \boldsymbol{\gamma}_h\|_{\boldsymbol{\Theta}'} + t \|\boldsymbol{\gamma} - \boldsymbol{\gamma}_h\|_0 \\ & \leq C \left(\sum_{T \in \mathcal{T}_h} \left(\eta_T^2 + h_T^2 (h_T^2 + t^2) \|g - g_h\|_{0,T}^2 \right) \right)^{1/2}, \end{aligned}$$

provided one is able to bound

$$(4.14) \quad |||(\tilde{\boldsymbol{\theta}}_h - \boldsymbol{\theta}_h, \tilde{w}_h - w_h)|||_h + \|\tilde{\boldsymbol{\gamma}}_h - \boldsymbol{\gamma}_h\|_{\boldsymbol{\Theta}'} + t \|\tilde{\boldsymbol{\gamma}}_h - \boldsymbol{\gamma}_h\|_0.$$

To this aim, we first notice that $\boldsymbol{\Theta}_h \times W_h \times \boldsymbol{\Gamma}_h \subset \tilde{\boldsymbol{\Theta}}_h \times \tilde{W}_h \times \tilde{\boldsymbol{\Gamma}}_h$. We need the following result, which states that functions in $\tilde{\boldsymbol{\Theta}}_h \times \tilde{W}_h$ can be approximated by functions in $\boldsymbol{\Theta}_h \times W_h$.

LEMMA 4.2. *Given $(\tilde{\boldsymbol{\eta}}, \tilde{v}) \in \tilde{\boldsymbol{\Theta}}_h \times \tilde{W}_h$, set $(\mathcal{I}\tilde{\boldsymbol{\eta}}, \mathcal{I}\tilde{v}) \in \boldsymbol{\Theta}_h \times W_h$, where \mathcal{I} denotes the usual Lagrange interpolating operator. Then it holds*

$$(4.15) \quad \begin{aligned} & \sum_{T \in \mathcal{T}_h} h_T^{-2} \left(\|\tilde{\boldsymbol{\eta}} - \mathcal{I}\tilde{\boldsymbol{\eta}}\|_{0,T}^2 + \frac{1}{h_T^2 + t^2} \|\tilde{v} - \mathcal{I}\tilde{v}\|_{0,T}^2 \right) \\ & + \sum_{E \in \mathcal{E}_h^i} h_E^{-1} \left(\|\tilde{\boldsymbol{\eta}} - \mathcal{I}\tilde{\boldsymbol{\eta}}\|_{0,E}^2 + \frac{1}{h_E^2 + t^2} \|\tilde{v} - \mathcal{I}\tilde{v}\|_{0,E}^2 \right) \leq C |||(\tilde{\boldsymbol{\eta}}, \tilde{v})|||_h^2. \end{aligned}$$

PROOF. Let $(\tilde{\boldsymbol{\eta}}, \tilde{v}) \in \tilde{\boldsymbol{\Theta}}_h \times \tilde{W}_h$ be given. By standard approximation results and scaling arguments, we have

$$(4.16) \quad \sum_{T \in \mathcal{T}_h} h_T^{-2} \|\tilde{\boldsymbol{\eta}} - \mathcal{I}\tilde{\boldsymbol{\eta}}\|_{0,T}^2 + \sum_{E \in \mathcal{E}_h^i} h_E^{-1} \|\tilde{\boldsymbol{\eta}} - \mathcal{I}\tilde{\boldsymbol{\eta}}\|_{0,E}^2 \leq C \|\tilde{\boldsymbol{\eta}}\|_1^2.$$

Furthermore, it holds

$$(4.17) \quad \begin{aligned} \|\tilde{v} - \mathcal{I}\tilde{v}\|_{0,T}^2 & \leq Ch_T^4 |\tilde{v}|_{2,T}^2 = Ch_T^4 |\nabla \tilde{v}|_{1,T}^2 \\ & \leq Ch_T^4 (|\nabla \tilde{v} - \tilde{\boldsymbol{\eta}}|_{1,T}^2 + |\tilde{\boldsymbol{\eta}}|_{1,T}^2). \end{aligned}$$

Using an inverse inequality we get

$$(4.18) \quad \|\tilde{v} - \mathcal{I}\tilde{v}\|_{0,T}^2 \leq Ch_T^2 \|\nabla \tilde{v} - \tilde{\boldsymbol{\eta}}\|_{0,T}^2 + Ch_T^4 |\tilde{\boldsymbol{\eta}}|_{1,T}^2.$$

Therefore, we obtain

$$\begin{aligned}
(4.19) \quad & \sum_{T \in \mathcal{T}_h} \frac{h_T^{-2}}{h_T^2 + t^2} \|\tilde{v} - \mathcal{I}\tilde{v}\|_{0,T}^2 \\
& \leq C \sum_{T \in \mathcal{T}_h} \frac{1}{h_T^2 + t^2} \|\nabla \tilde{v} - \tilde{\boldsymbol{\eta}}\|_{0,T}^2 + C \sum_{T \in \mathcal{T}_h} \frac{h_T^2}{h_T^2 + t^2} |\tilde{\boldsymbol{\eta}}|_{1,T}^2 \\
& \leq C \left(\sum_{T \in \mathcal{T}_h} \frac{1}{h_T^2 + t^2} \|\nabla \tilde{v} - \tilde{\boldsymbol{\eta}}\|_{0,T}^2 + \|\tilde{\boldsymbol{\eta}}\|_1^2 \right) \\
& \leq C \|(\tilde{\boldsymbol{\eta}}, \tilde{v})\|_h^2.
\end{aligned}$$

The shape regularity of \mathcal{T}_h , scaling arguments, and estimate (4.19) show that

$$(4.20) \quad \sum_{E \in \mathcal{E}_h^i} \frac{h_E^{-1}}{h_E^2 + t^2} \|\tilde{v} - \mathcal{I}\tilde{v}\|_{0,E}^2 \leq C \sum_{T \in \mathcal{T}_h} \frac{h_T^{-2}}{h_T^2 + t^2} \|\tilde{v} - \mathcal{I}\tilde{v}\|_{0,T}^2 \leq C \|(\tilde{\boldsymbol{\eta}}, \tilde{v})\|_h^2.$$

Collecting (4.16), (4.19) and (4.20) gives the estimate (4.15). \square

We are now ready to prove the following proposition.

PROPOSITION 4.3. *We have*

$$(4.21) \quad \begin{aligned}
& \|(\tilde{\boldsymbol{\theta}}_h - \boldsymbol{\theta}_h, \tilde{w}_h - w_h)\|_h + \|\tilde{\boldsymbol{\gamma}}_h - \boldsymbol{\gamma}_h\|_{\boldsymbol{\Theta}'} + t \|\tilde{\boldsymbol{\gamma}}_h - \boldsymbol{\gamma}_h\|_0 \\
& \leq C \left(\sum_{T \in \mathcal{T}_h} \left(\eta_T^2 + h_T^2 (h_T^2 + t^2) \|g - g_h\|_{0,T}^2 \right) \right)^{1/2}.
\end{aligned}$$

PROOF. Consider $(\tilde{\boldsymbol{\theta}}_h - \boldsymbol{\theta}_h, \tilde{w}_h - w_h; \tilde{\boldsymbol{\gamma}}_h - \boldsymbol{\gamma}_h) \in \tilde{\boldsymbol{\Theta}}_h \times \tilde{W}_h \times \tilde{\boldsymbol{\Gamma}}_h$. The discrete stability for the $(k+1)$ -th Falk-Tu element (see Proposition 3.2) implies that there exists $(\tilde{\boldsymbol{\eta}}, \tilde{v}; \tilde{\boldsymbol{\tau}})$ in $\tilde{\boldsymbol{\Theta}}_h \times \tilde{W}_h \times \tilde{\boldsymbol{\Gamma}}_h$ such that

$$(4.22) \quad \|(\tilde{\boldsymbol{\eta}}, \tilde{v})\|_h + \|\tilde{\boldsymbol{\tau}}\|_h \leq 1$$

and

$$\begin{aligned}
(4.23) \quad & C \left(\|(\tilde{\boldsymbol{\theta}}_h - \boldsymbol{\theta}_h, \tilde{w}_h - w_h)\|_h + \|\tilde{\boldsymbol{\gamma}}_h - \boldsymbol{\gamma}_h\|_h \right) \\
& \leq \left\{ a(\tilde{\boldsymbol{\theta}}_h - \boldsymbol{\theta}_h, \tilde{\boldsymbol{\eta}}) + (\tilde{\boldsymbol{\gamma}}_h - \boldsymbol{\gamma}_h, \nabla \tilde{v} - \tilde{\boldsymbol{\eta}}) \right\} \\
& \quad + \left\{ -(\nabla(\tilde{w}_h - w_h) - (\tilde{\boldsymbol{\theta}}_h - \boldsymbol{\theta}_h), \tilde{\boldsymbol{\tau}}) + \mu^{-1} t^2 (\tilde{\boldsymbol{\gamma}}_h - \boldsymbol{\gamma}_h, \tilde{\boldsymbol{\tau}}) \right\} \\
& = I + II.
\end{aligned}$$

On one hand, since $(\tilde{\boldsymbol{\theta}}_h, \tilde{w}_h; \tilde{\boldsymbol{\gamma}}_h)$ (respectively $(\boldsymbol{\theta}_h, w_h; \boldsymbol{\gamma}_h)$) solves the higher-order (low-order) discrete problem, we have

$$\begin{aligned}
(4.24) \quad & I = a(\tilde{\boldsymbol{\theta}}_h - \boldsymbol{\theta}_h, \tilde{\boldsymbol{\eta}}) + (\tilde{\boldsymbol{\gamma}}_h - \boldsymbol{\gamma}_h, \nabla \tilde{v} - \tilde{\boldsymbol{\eta}}) \\
& = (g, \tilde{v}) - a(\boldsymbol{\theta}_h, \tilde{\boldsymbol{\eta}}) - (\boldsymbol{\gamma}_h, \nabla \tilde{v} - \tilde{\boldsymbol{\eta}}) \\
& = (g, \tilde{v} - \mathcal{I}\tilde{v}) - a(\boldsymbol{\theta}_h, \tilde{\boldsymbol{\eta}} - \mathcal{I}\tilde{\boldsymbol{\eta}}) - (\boldsymbol{\gamma}_h, \nabla(\tilde{v} - \mathcal{I}\tilde{v}) - (\tilde{\boldsymbol{\eta}} - \mathcal{I}\tilde{\boldsymbol{\eta}})),
\end{aligned}$$

where $\mathcal{I}\tilde{\boldsymbol{\eta}} \in \boldsymbol{\Theta}_h$ and $\mathcal{I}\tilde{v} \in W_h$ are as in Lemma 4.2. An elementwise integration by parts gives

$$(4.25) \quad \begin{aligned} I &= \sum_{T \in \mathcal{T}_h} \left\{ \int_T (\mathbf{div} \mathbf{C}\boldsymbol{\varepsilon}(\boldsymbol{\theta}_h) + \boldsymbol{\gamma}_h) \cdot (\tilde{\boldsymbol{\eta}} - \mathcal{I}\tilde{\boldsymbol{\eta}}) - \int_{\partial T} \mathbf{C}\boldsymbol{\varepsilon}(\boldsymbol{\theta}_h) \mathbf{n} \cdot (\tilde{\boldsymbol{\eta}} - \mathcal{I}\tilde{\boldsymbol{\eta}}) \right\} \\ &\quad + \sum_{T \in \mathcal{T}_h} \left\{ \int_T (\mathbf{div} \boldsymbol{\gamma}_h + g) (\tilde{v} - \mathcal{I}\tilde{v}) - \int_{\partial T} \boldsymbol{\gamma}_h \cdot \mathbf{n} (\tilde{v} - \mathcal{I}\tilde{v}) \right\} \end{aligned}$$

by which

$$(4.26) \quad \begin{aligned} I &= \sum_{T \in \mathcal{T}_h} \int_T (\mathbf{div} \mathbf{C}\boldsymbol{\varepsilon}(\boldsymbol{\theta}_h) + \boldsymbol{\gamma}_h) \cdot (\tilde{\boldsymbol{\eta}} - \mathcal{I}\tilde{\boldsymbol{\eta}}) - \sum_{E \in \mathcal{E}_h} \int_E \llbracket \mathbf{C}\boldsymbol{\varepsilon}(\boldsymbol{\theta}_h) \mathbf{n} \rrbracket \cdot (\tilde{\boldsymbol{\eta}} - \mathcal{I}\tilde{\boldsymbol{\eta}}) \\ &\quad + \sum_{T \in \mathcal{T}_h} \int_T (\mathbf{div} \boldsymbol{\gamma}_h + g) (\tilde{v} - \mathcal{I}\tilde{v}) - \sum_{E \in \mathcal{E}_h} \int_E \llbracket \boldsymbol{\gamma}_h \cdot \mathbf{n} \rrbracket (\tilde{v} - \mathcal{I}\tilde{v}). \end{aligned}$$

Hence, recalling the boundary conditions in (2.3), and denoting $\mathcal{E}_h^{IFS} = \mathcal{E}_h^I \cup \mathcal{E}_h^F \cup \mathcal{E}_h^S$ and $Eh^{IF} = \mathcal{E}_h^I \cup \mathcal{E}_h^F$ it holds

$$(4.27) \quad \begin{aligned} I &\leq C \left[\left(\sum_{T \in \mathcal{T}_h} h_T^2 \|\mathbf{div} \mathbf{C}\boldsymbol{\varepsilon}(\boldsymbol{\theta}_h) + \boldsymbol{\gamma}_h\|_{0,T}^2 \right)^{1/2} \left(\sum_{T \in \mathcal{T}_h} h_T^{-2} \|\tilde{\boldsymbol{\eta}} - \mathcal{I}\tilde{\boldsymbol{\eta}}\|_{0,T}^2 \right)^{1/2} \right. \\ &\quad + \left(\sum_{E \in \mathcal{E}_h^{IFS}} h_E \|\llbracket \mathbf{C}\boldsymbol{\varepsilon}(\boldsymbol{\theta}_h) \mathbf{n} \rrbracket\|_{0,E}^2 \right)^{1/2} \left(\sum_{E \in \mathcal{E}_h^{IFS}} h_E^{-1} \|\tilde{\boldsymbol{\eta}} - \mathcal{I}\tilde{\boldsymbol{\eta}}\|_{0,E}^2 \right)^{1/2} \\ &\quad + \left(\sum_{E \in \mathcal{E}_h^H} h_E \|\llbracket (\mathbf{C}\boldsymbol{\varepsilon}(\boldsymbol{\theta}_h) \mathbf{n}) \cdot \mathbf{n} \rrbracket\|_{0,E}^2 \right)^{1/2} \left(\sum_{E \in \mathcal{E}_h^H} h_E^{-1} \|(\tilde{\boldsymbol{\eta}} - \mathcal{I}\tilde{\boldsymbol{\eta}}) \cdot \mathbf{n}\|_{0,E}^2 \right)^{1/2} \\ &\quad + \left(\sum_{T \in \mathcal{T}_h} h_T^2 (h_T^2 + t^2) \|\mathbf{div} \boldsymbol{\gamma}_h + g\|_{0,T}^2 \right)^{1/2} \left(\sum_{T \in \mathcal{T}_h} \frac{1}{h_T^2 (h_T^2 + t^2)} \|\tilde{v} - \mathcal{I}\tilde{v}\|_{0,T}^2 \right)^{1/2} \\ &\quad \left. + \left(\sum_{E \in \mathcal{E}_h^{IF}} h_E (h_E^2 + t^2) \|\llbracket \boldsymbol{\gamma}_h \cdot \mathbf{n} \rrbracket\|_{0,E}^2 \right)^{1/2} \left(\sum_{E \in \mathcal{E}_h^{IF}} \frac{1}{h_E (h_E^2 + t^2)} \|\tilde{v} - \mathcal{I}\tilde{v}\|_{0,E}^2 \right)^{1/2} \right]. \end{aligned}$$

Using Lemma 4.2, we get

$$(4.28) \quad \begin{aligned} I &\leq C \left[\left(\sum_{T \in \mathcal{T}_h} h_T^2 \|\mathbf{div} \mathbf{C}\boldsymbol{\varepsilon}(\boldsymbol{\theta}_h) + \boldsymbol{\gamma}_h\|_{0,T}^2 \right)^{1/2} + \left(\sum_{E \in \mathcal{E}_h^I \cup \mathcal{E}_h^F \cup \mathcal{E}_h^S} h_E \|\llbracket \mathbf{C}\boldsymbol{\varepsilon}(\boldsymbol{\theta}_h) \mathbf{n} \rrbracket\|_{0,E}^2 \right)^{1/2} \right. \\ &\quad + \left(\sum_{E \in \mathcal{E}_h^H} h_E \|\llbracket (\mathbf{C}\boldsymbol{\varepsilon}(\boldsymbol{\theta}_h) \mathbf{n}) \cdot \mathbf{n} \rrbracket\|_{0,E}^2 \right)^{1/2} + \left(\sum_{T \in \mathcal{T}_h} h_T^2 (h_T^2 + t^2) \|\mathbf{div} \boldsymbol{\gamma}_h + g\|_{0,T}^2 \right)^{1/2} \\ &\quad \left. + \left(\sum_{E \in \mathcal{E}_h^I \cup \mathcal{E}_h^F} h_E (h_E^2 + t^2) \|\llbracket \boldsymbol{\gamma}_h \cdot \mathbf{n} \rrbracket\|_{0,E}^2 \right)^{1/2} \right] \|(\tilde{\boldsymbol{\eta}}, \tilde{v})\|_h. \end{aligned}$$

On the other hand, since $(\tilde{\boldsymbol{\theta}}_h, \tilde{w}_h; \tilde{\boldsymbol{\gamma}}_h)$ solves the higher-order discrete problem,

we have

$$\begin{aligned}
(4.29) \quad II &= -(\nabla(\tilde{w}_h - w_h) - (\tilde{\boldsymbol{\theta}}_h - \boldsymbol{\theta}_h), \tilde{\boldsymbol{\tau}}) + \mu^{-1}t^2(\tilde{\boldsymbol{\gamma}}_h - \boldsymbol{\gamma}_h, \tilde{\boldsymbol{\tau}}) \\
&= -(\mu^{-1}t^2\boldsymbol{\gamma}_h - (\nabla w_h - \boldsymbol{\theta}_h), \tilde{\boldsymbol{\tau}}) \\
&\leq \left(\sum_{T \in \mathcal{T}_h} \frac{1}{h_T^2 + t^2} \|\mu^{-1}t^2\boldsymbol{\gamma}_h - (\nabla w_h - \boldsymbol{\theta}_h)\|_{0,T}^2 \right)^{1/2} \left(\sum_{T \in \mathcal{T}_h} (h_T^2 + t^2) \|\tilde{\boldsymbol{\tau}}\|_{0,T}^2 \right)^{1/2}.
\end{aligned}$$

As a consequence, from (4.23), (4.28), (4.29), using (4.22) and recalling definitions (4.2)–(4.4), a triangle inequality gives

$$\begin{aligned}
(4.30) \quad & \|(\tilde{\boldsymbol{\theta}}_h - \boldsymbol{\theta}_h, \tilde{w}_h - w_h)\|_h + \|\tilde{\boldsymbol{\gamma}}_h - \boldsymbol{\gamma}_h\|_h \\
& \leq C \left(\sum_{T \in \mathcal{T}_h} (\eta_T^2 + h_T^2(h_T^2 + t^2)\|g - g_h\|_{0,T}^2) \right)^{1/2}.
\end{aligned}$$

The "Pitkäranta-Verfürth trick", applied to $\tilde{\boldsymbol{\gamma}}_h - \boldsymbol{\gamma}_h$, gives (cf. (3.20))

$$(4.31) \quad \|\tilde{\boldsymbol{\gamma}}_h - \boldsymbol{\gamma}_h\|_{\Theta'} \leq C \left(\|\tilde{\boldsymbol{\gamma}}_h - \boldsymbol{\gamma}_h\|_h + \|\tilde{\boldsymbol{\theta}}_h - \boldsymbol{\theta}_h\|_1 \right).$$

Combining (4.30) and (4.31) we get estimate (4.21). The proof is complete. \square

5 Numerical results

In the present section we numerically test the behavior of the error estimator η given by (4.5). For comparison purposes, we will consider the true error

$$(5.1) \quad e_N = (\|(\boldsymbol{\theta} - \boldsymbol{\theta}_h, w - w_h)\|_h^2 + \|\boldsymbol{\gamma} - \boldsymbol{\gamma}_h\|_h^2)^{1/2},$$

where the index N represents the number of degrees of freedom, and the norms in the right-hand side has been introduced in (3.4) and (3.6). The a-priori convergence result for the error e_N has been proved in Section 2. For simplicity, we restrict our study to the lowest order element in the Falk-Tu family, i.e. to the choice $k = 1$ in (2.10)–(2.12).

In the sequel we will consider both uniform and adaptively refined families of meshes, generated by using MATLAB[®]. Given a starting coarse grid, a uniform mesh family is obtained by a classical triangle subdivision: a mesh refinement is generated by dividing all the elements into four sub-triangles using a standard edge bisection procedure.

The adaptively refined family is obtained starting from a coarse mesh, and adopting the following standard strategy:

- (1) Calculate the local element error indicators η_i , $i = 1, \dots, M$, where M is the number of elements in the mesh.
- (2) Mark for refinement the elements T_j such that

$$\eta_j \geq \frac{1}{2} \max_{i=1, \dots, M} \eta_i, \quad j = 1, \dots, M.$$

(3) Generate the refined mesh using a red-green-blue strategy, as shown for instance in [41]. Essentially, each element marked for refinement is divided into four subtriangles, and suitable additional subdivisions are performed in order to avoid hanging nodes and degenerate elements. Furthermore, at each adaptive refinement step the mesh is jiggled by slightly adjusting the positions of the nodes, in order to increase the quality of the resulting grid.

As a preliminary test we consider a clamped homogeneous and isotropic square plate problem, for which the analytical (regular) solution is available (see [21] for all the details). In Figure 5.1 we plot the error e_N as a function of the number of degrees of freedom N for a family of uniform meshes and for different values of the thickness t . Note that we clearly have $N \sim h^{-2}$. Therefore, due to the regularity of the solution and the results of Section 2, we expect a convergence rate of order $O(h) \sim O(N^{-\frac{1}{2}})$ for all thickness choices. The numerical results fully agree with this theoretical prediction.

5.1 *L-shaped plate with constant load*

We consider an L-shaped plate, where the domain Ω is obtained carving out the upper right quarter of a $[-1, 1] \times [-1, 1]$ square. The applied load is a constant function $g = 1$ and the material constants are $E = 10.92$ and $\nu = 0.3$. In Figure 5.2 we show the initial coarse mesh we have always used for both the uniform and the adaptive refinements. We focus on the following two cases.

5.1.1 *Clamped corner case*

The plate is clamped along the two edges forming the re-entrant corner, while it is free on the other edges. The analytical solution to this problem is not known, therefore our tests will be restricted to the error indicator η_N . Nevertheless, on the basis of the results for Kirchhoff plates found in [10] and [33], we expect the best Sobolev regularity of the analytical rotation $\boldsymbol{\theta}$ near the re-entrant corner to be $H^{3/2}$, while the deflection w is more regular. As a consequence, Proposition 3.3 and standard polynomial interpolation results suggest a convergence rate

$$(5.2) \quad e_N \sim h^{1/2} \sim N^{-\frac{1}{4}}$$

for uniformly refined meshes.

In Figures 5.3 and 5.4 we plot the error estimator η_N as a function of N , for varying thicknesses, respectively for uniform and adaptively refined meshes. While the uniformly refined strategy exhibits a slow convergence rate as expected, the adaptively refined procedure clearly displays better performances. In Figure 5.5 we plot a comparison between the two refinement strategies for the choices $t = 10^{-2}$ and $t = 10^{-4}$; the superior performance of the adaptively refined meshes, in terms of error versus degrees of freedom, can be noticed.

In Figure 5.6 we show two meshes obtained at different stages of refinement, for both the choices $t = 10^{-2}$ and $t = 10^{-4}$. Looking at the refined meshes, the error indicator succeeds in detecting the solution irregularity around the re-entrant corner.

5.1.2 Free corner case

The plate is now free along the two edges forming the re-entrant corner, while it is clamped on the other edges. Again, the analytical solution to this problem is not available, so that only the error estimator η_N is studied. However, from the Kirchhoff plate results of [10] and [33], we expect the best Sobolev regularity of the analytical rotation θ near the re-entrant corner to be $H^{1.63}$, while the deflection w is more regular. As a consequence, this case is slightly more favorable than the previous one, from the geometric singularity viewpoint.

In Figures 5.7 and 5.8 we plot the error estimator η_N as a function of N , for varying thicknesses, respectively for uniform and adaptively refined meshes. In Figure 5.9 we plot a comparison between the two refinement strategies for the choices $t = 10^{-2}$ and $t = 10^{-4}$. The procedures give analogous results: this can be probably explained by noticing that also the uniform refinements exhibit the optimal $O(N^{-1/2})$ convergence rate. In Figure 5.10 we show two meshes obtained at different stages of refinement, for both the choices $t = 10^{-2}$ and $t = 10^{-4}$.

5.2 Semi-infinite plate: a boundary layer test

Boundary layers are an important issue in Reissner-Mindlin plate analysis, see for instance [3, 23, 35, 6, 20]. We consider the bending problem of a semi-infinite plate introduced in [2]. The midsurface and the boundary of the plate, respectively, are described by the sets

$$(5.3) \quad \Omega = \{(x, y) \in \mathbb{R}^2 | y > 0\} \quad \text{and} \quad \Gamma = \{(x, y) \in \mathbb{R}^2 | y = 0\}.$$

The plate is assumed to be free on the boundary Γ and subjected to a cosine type transverse loading $g = \frac{\cos x}{2(1+\nu)}$. Our choice for the thickness and material parameters are $t = 10^{-2}$, $\nu = 0.3$, $E = 1$. The analytical x -periodic solution of this problem is given in [2] and not reported here. Such a solution presents a boundary layer generated by the free edge Γ . Therefore, the present problem can be used to analyze both the effectivity of our estimator and its ability to detect the error arising from the edge effects.

We solve the problem with the lowest-order Falk-Tu element on the subdomain $D = (0, \pi/2) \times (0, 3\pi/2)$; along the boundaries $x = 0$, $x = \pi/2$ and $x = 3\pi/2$ we impose the Dirichlet boundary conditions resulting from the exact solution. In Figure 5.11 we show the initial coarse mesh we have used for both the uniform and the adaptive refinements.

Figure 5.12 displays the convergence history of the error and of the error estimator on the subdomain $D_b = \{(x, y) \in D | y \in (0, \pi/2)\}$, for both the uniform and the adaptive refinement strategies. The two considered quantities exhibit a similar behaviour, as it can be deduced also by Figure 5.13, which reports the effectivity index corresponding to the adaptive meshes. Furthermore, in Figure 5.14 we show two meshes obtained at different stages of adaptive refinement.

Finally, in Figures 5.15 and 5.16 we plot the local error and the error estimator distribution, element by element on the subdomain D_b previously introduced.

Two uniform meshes are here considered, corresponding to a coarse and a fine grid, respectively. In both cases the presence of the layer causes higher local errors near the free boundary, as it can be appreciated in the above indicated plots. The figures show that also the error estimator attains higher values in the elements near the free boundary, and its distribution pattern is very similar to the one of the true error. As a consequence, this test confirms that the error indicator is able to detect boundary layers.

REFERENCES

1. D.N. Arnold and R.S. Falk, *A uniformly accurate finite element method for the Reissner-Mindlin plate*, SIAM J. Numer. Anal. **26** (1989), pp. 1276–1290.
2. D.N. Arnold and R.S. Falk, *Edge effects in the Reissner-Mindlin plate theory*, in A.K. Noor, T. Belytschko, and J.C. Simo, editors, *Analytical and Computational Models of Shells*, pages 71–90, New York (1989), ASME.
3. D.N. Arnold and R.S. Falk, *Asymptotic analysis of the boundary layer for the Reissner-Mindlin plate model*, SIAM J. Numer. Anal. **27** (1996), pp. 486–514.
4. F. Auricchio and C. Lovadina, *Partial selective reduced integration schemes and kinematically linked interpolations for plate bending problems*, Math. Models Methods Appl. Sci. **9** (1999), pp. 693–722.
5. F. Auricchio and C. Lovadina, *Analysis of kinematic linked interpolation methods for Reissner-Mindlin plate problems*, Comput. Methods Appl. Mech. Engrg. **190** (2001), pp. 2465–2482.
6. L. Beirão da Veiga, *Finite element methods for a modified Reissner-Mindlin free plate model*, SIAM J. Numer. Anal. **42** (2004), pp. 1572–1591.
7. L. Beirão da Veiga, J. Niiranen and R. Stenberg *A posteriori error estimates for the plate bending Morley element*, Numer. Math. **106** (2007), pp 165–179.
8. L. Beirão da Veiga, J. Niiranen and R. Stenberg *A family of C^0 finite elements for Kirchhoff plates I: theoretical analysis*, SIAM J. Numer. Anal. **45** (2007), pp 2047–2071.
9. L. Beirão da Veiga, J. Niiranen and R. Stenberg *A family of C^0 finite elements for Kirchhoff plates II: numerical tests*, Comput. Methods Appl. Mech. Engrg. **197** (2008), pp 1850–1864.
10. H. Blum and R. Rannacher, *On the boundary value problem of the biharmonic operator on domains with angular corners*, Math. Meth. Appl. Sci. **2** (1980), pp. 556–581.
11. D. Braess and R. Verfürth *A posteriori error estimators for the Raviart-Thomas element*, SIAM J. Numer. Anal. **33** (1996), pp. 2431–2444.
12. F. Brezzi, K.J. Bathe and M. Fortin, *Mixed-interpolated elements for Reissner-Mindlin plates*, Internat. J. Numer. Methods Engrg. **28** (1989), pp. 1787–1801.
13. F. Brezzi and M. Fortin, *Mixed and Hybrid Finite Element Methods*, Springer, New York, 1991.
14. F. Brezzi, M. Fortin and R. Stenberg, *Error analysis of mixed-interpolated elements for Reissner-Mindlin plates*, Math. Models Methods Appl. Sci. **1** (1991), pp. 125–151.
15. C. Carstensen, *Residual-based a posteriori error estimate for a nonconforming Reissner-Mindlin plate finite element*, SIAM J. Numer. Anal. **39** (2002), pp. 2034–2044.

16. C. Carstensen and J. Hu, *A posteriori error analysis for conforming MITC elements for Reissner-Mindlin Plate*, Math. Comp. **77** (2008), pp. 611–632.
17. C. Carstensen and J. Schöberl, *Residual-based a posteriori error estimate for a mixed Reissner–Mindlin plate finite element*, Numer.Math. **103** (2006), pp. 225–250.
18. D. Chapelle and R. Stenberg, *An optimal low-order locking-free finite element method for Reissner-Mindlin plates*, Math. Models and Methods in Appl. Sci., **8** (1998), pp. 407–430.
19. D. Chapelle and R. Stenberg *Stabilized finite element formulations for shells in a bending dominated state*, SIAM J. Numer. Anal. **36** (1999), pp. 32–73.
20. C. Chinosi, *PSRI elements for the Reissner–Mindlin free plate*, Comp. & Struct., **83** (2005), pp. 2559–2572.
21. C. Chinosi and C. Lovadina, *Numerical analysis of some mixed finite element methods for Reissner-Mindlin plates*, Comput. Mechanics, **16** (1995), pp. 36–44.
22. P.G. Ciarlet, *The Finite Element Method for Elliptic Problems*, North-Holland, 1978.
23. P. Destuynder and M. Salaun, *Mathematical Analysis of Thin Plate Models*, Springer-Verlag, Berlin, 1996.
24. R. Duran and E. Liberman, *On mixed finite-element methods for the Reissner-Mindlin plate model*, Math. Comp. **58** (1992), pp. 561–573.
25. R.S. Falk and T. Tu, *Locking-free finite elements for the Reissner-Mindlin plate*, Math. Comp., **69** (2000), pp. 911–928.
26. E. Liberman, *A posteriori error estimator for a mixed finite element method for Reissner-Mindlin plate*, Math. Comp. **70** (2000), pp. 1383–1396.
27. C. Lovadina, *A new class of mixed finite element methods for Reissner-Mindlin plates*, SIAM J. Numer. Anal. **33** (1996), pp. 2457–2467.
28. C. Lovadina, *Analysis of a mixed finite element method for the Reissner-Mindlin plate problems*, Comput. Methods Appl. Mech. Engrg. **163** (1998), pp. 71–85.
29. C. Lovadina and R. Stenberg, *A posteriori error analysis of the Linked Interpolation Technique for plate bending problems*, SIAM J. Numer. Anal. **43** (2005), pp. 2227–2249.
30. M. Lyly, *On the connection between some linear triangular Reissner-Mindlin plate bending elements*, Numer. Math. **85** (2000), pp. 77–107.
31. M. Lyly, J. Niiranen and R. Stenberg, *A refined error analysis of MITC plate elements*, Math. Models Methods Appl. Sci. **16** (2006), pp 967–977.
32. M. Lyly and R. Stenberg, *Stabilized finite element methods for Reissner-Mindlin plates*, Forschungsbericht 4, Universität Innsbruck, Institut für Mathematik und Geometrie, (1999).
33. H. Melzer and R. Rannacher, *Spannungskonzentrationen in Eckpunkten der vertikal belasteten Kirchhoffschen Platte*, Bauingenieur **55** (1980), pp. 181–189.
34. J. Pitkäranta, *Boundary subspaces for the finite element method with Lagrange multipliers*, Numer. Math. **33** (1979), pp. 273–289.
35. J. Pitkäranta and M. Suri, *Design principles and error analysis for reduced-shear plate-bending finite elements*, **75** (1996), pp. 223–266.
36. R. Stenberg, *A new finite element formulation for the plate bending problem*, in **Asymptotic Methods for Elastic Structures**, eds. P.G. Ciarlet, L. Trabucho and J. Viaño, Walter de Gruyter & Co.,

37. R.L. Taylor and F. Auricchio, *Linked interpolation for Reissner-Mindlin plate elements: Part II- A simple triangle*, Int. J. Numer. Methods Eng. **36** (1993), pp. 3057–3066.
38. A. Tessler and T.J.R. Hughes, *A three-node Mindlin plate element with improved transverse shear*, Comput. Methods Appl. Mech. Engrg. **50** (1985), pp. 71–101.
39. R. Verfürth, *Error estimates for a finite element approximation of the Stokes problem*, RAIRO Anal. Numer. **18** (1984), pp. 175–182.
40. R. Verfürth, *A posteriori error estimation and adaptive mesh-refinement techniques*, J. Comput. Appl. Math. **50** (1994), pp. 67–83.
41. R. Verfürth, *A Review of a Posteriori Error Estimation and Adaptive Mesh-Refinement Techniques*, Teubner Verlag and J. Wiley, Stuttgart, 1996.
42. R. Verfürth, *Robust a posteriori error estimators for singularly perturbed reaction-diffusion equations*, Numer.Math. **78** (1998), pp. 479–493.

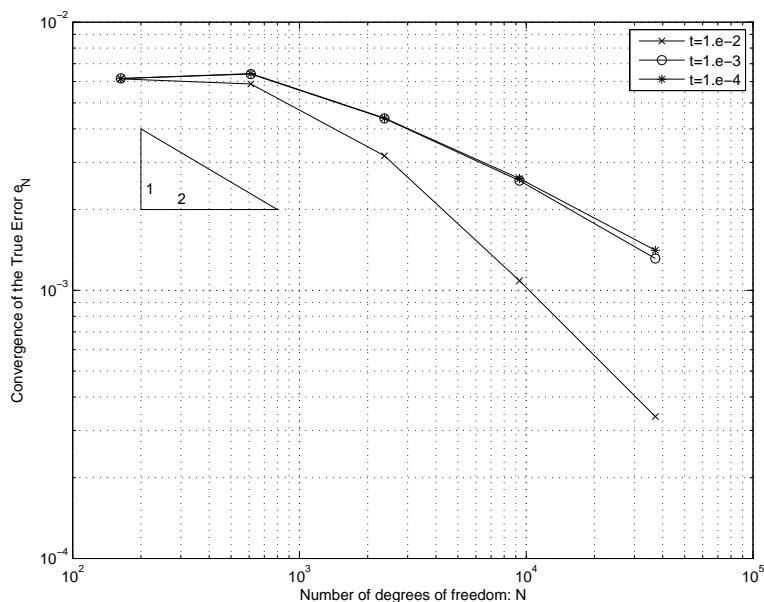


Figure 5.1: Square plate: convergence of the error for uniform refinements, $t = 10^{-2} \div 10^{-4}$

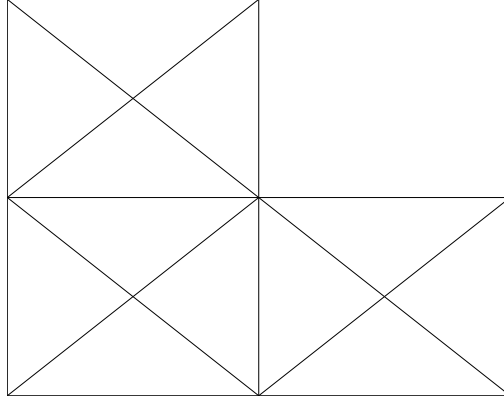
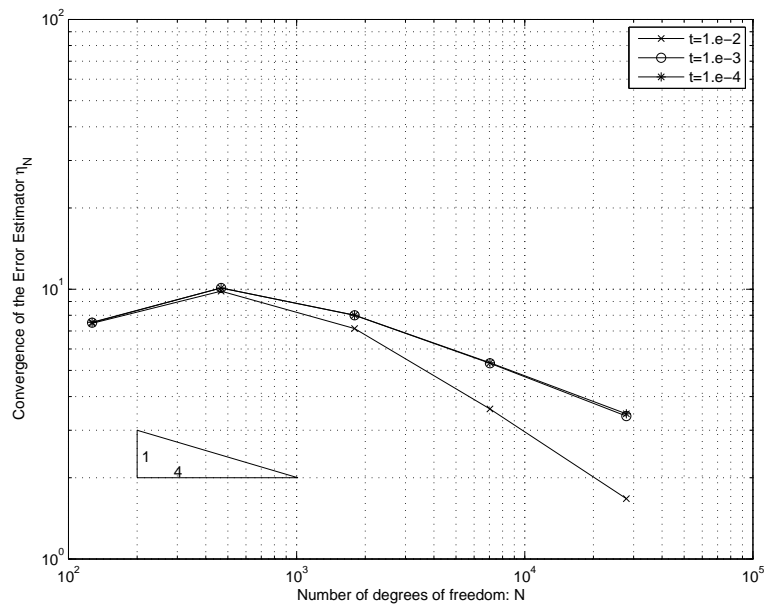


Figure 5.2: L-shaped plate: initial mesh.

Figure 5.3: L-shaped plate, clamped corner: convergence of the error estimator for uniform refinements, $t = 10^{-2} \div 10^{-4}$

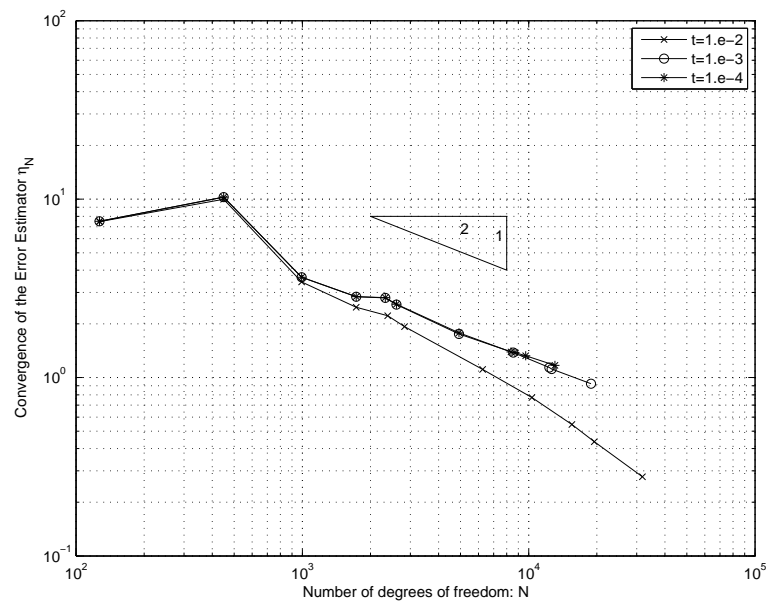


Figure 5.4: L-shaped plate, clamped corner: convergence of the error estimator for adaptive refinements, $t = 10^{-2} \div 10^{-4}$

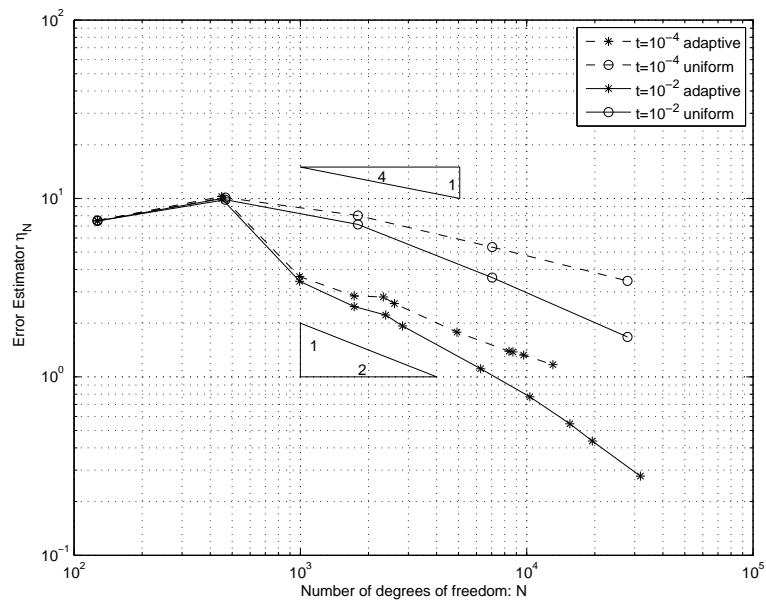


Figure 5.5: L-shaped plate, clamped corner: convergence of the error estimator for uniform and adaptive refinements, $t = 10^{-2}$ (solid line) and $t = 10^{-4}$ (dashed line)

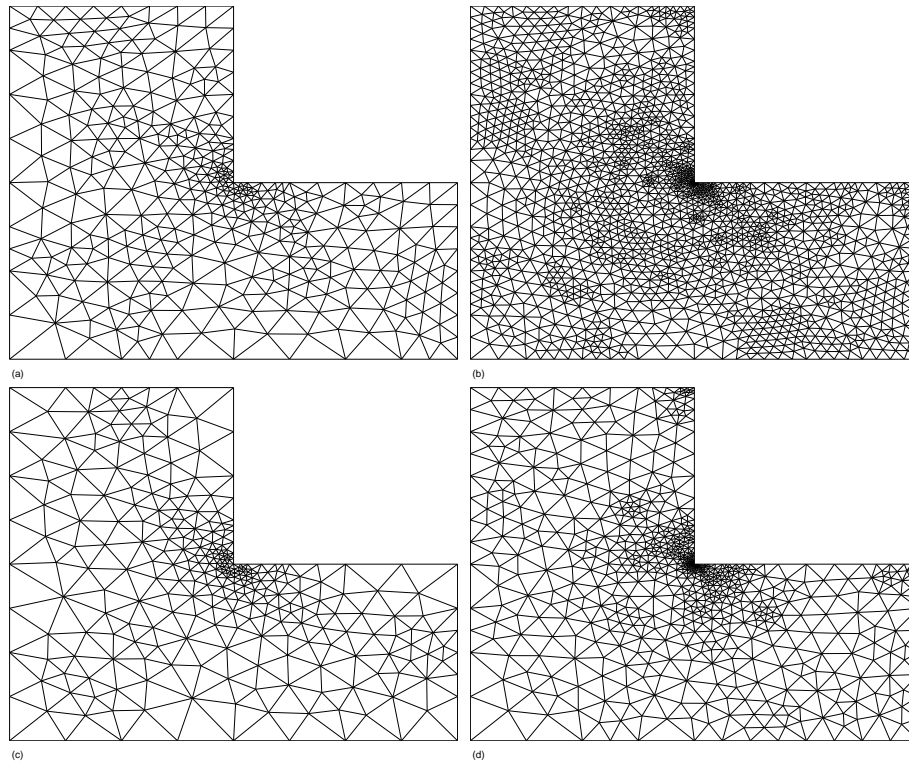


Figure 5.6: L-shaped plate, clamped corner: (a)-(b) seventh refinement step $N=6261$, and eleventh refinement step $N=31796$, for $t = 10^{-2}$; (c)-(d) seventh refinement step $N=4923$, and eleventh refinement step $N=13069$, for $t = 10^{-4}$

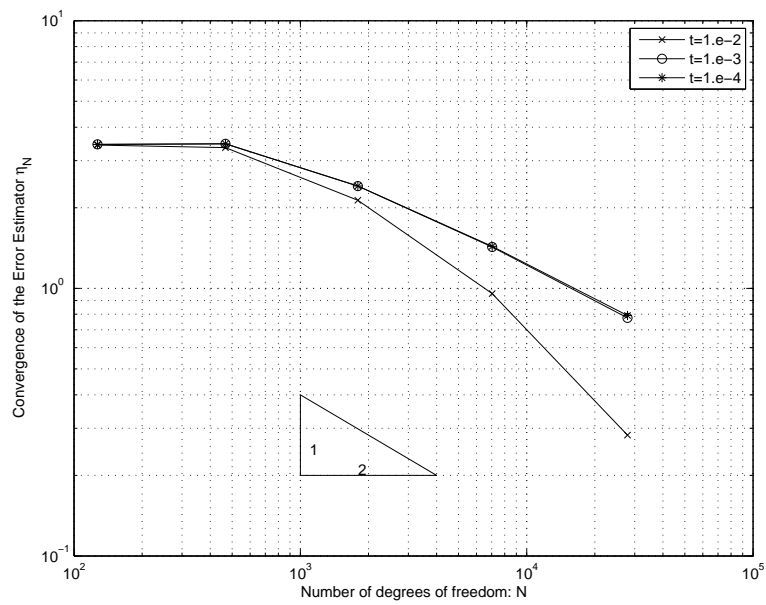


Figure 5.7: L-shaped plate, free corner: convergence of the error estimator for uniform refinements, $t = 10^{-2} \div 10^{-4}$

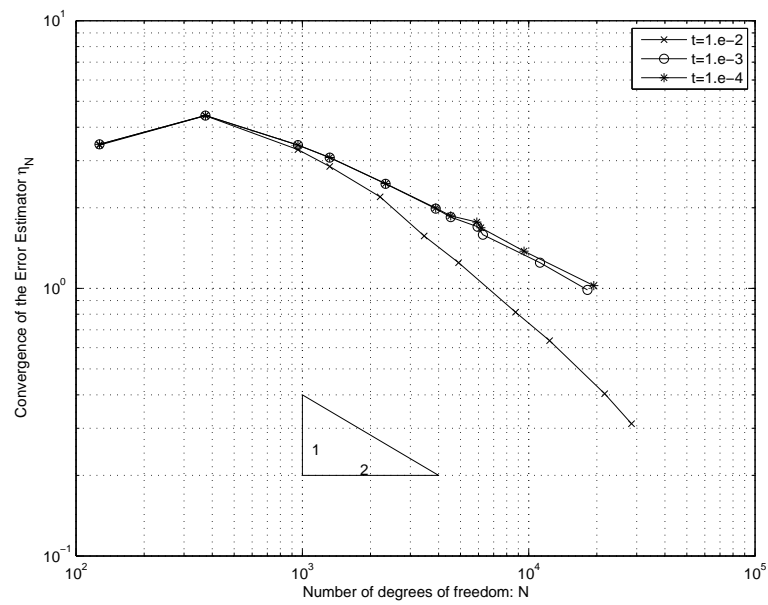


Figure 5.8: L-shaped plate, free corner: convergence of the error estimator for adaptive refinements, $t = 10^{-2} \div 10^{-4}$

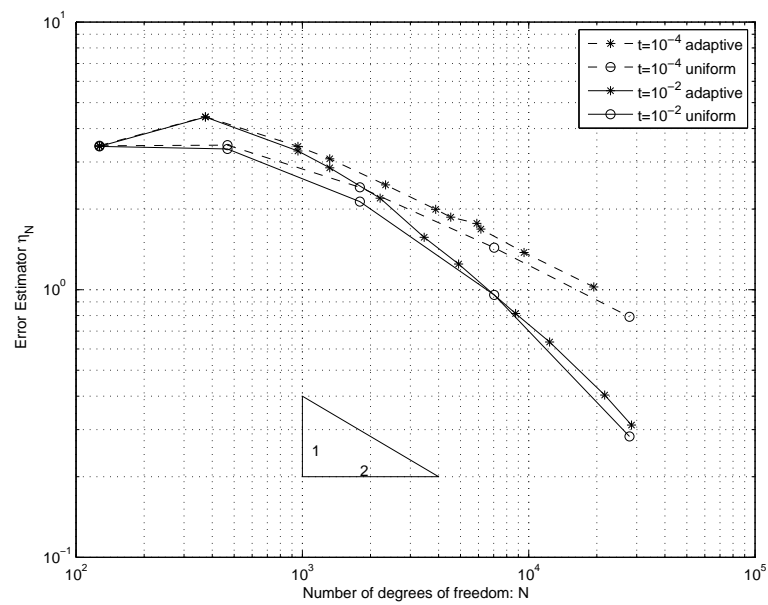


Figure 5.9: L-shaped plate, free corner: convergence of the error estimator for uniform and adaptive refinements, $t = 10^{-2}$ (solid line) and $t = 10^{-4}$ (dashed line)

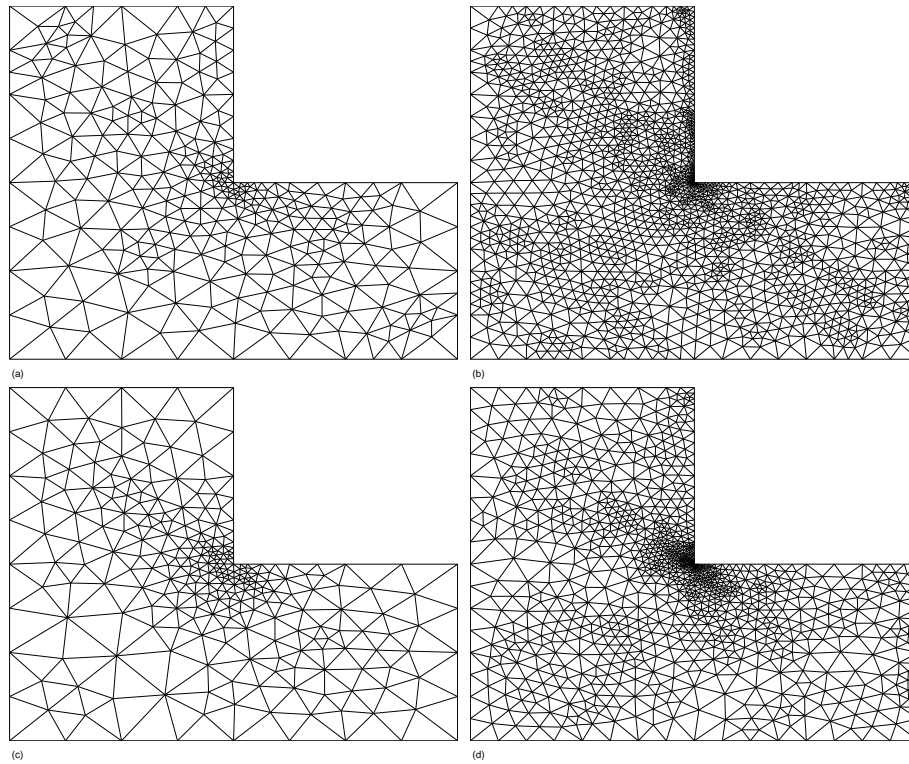


Figure 5.10: L-shaped plate, free corner: (a)-(b) seventh refinement step $N=4902$, and eleventh refinement step $N=28489$, for $t = 10^{-2}$; (c)-(d) seventh refinement step $N=4526$, and eleventh refinement step $N=19404$, for $t = 10^{-4}$

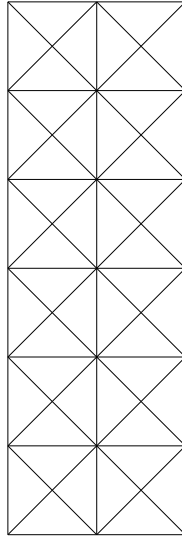


Figure 5.11: Semi-infinite plate: initial mesh

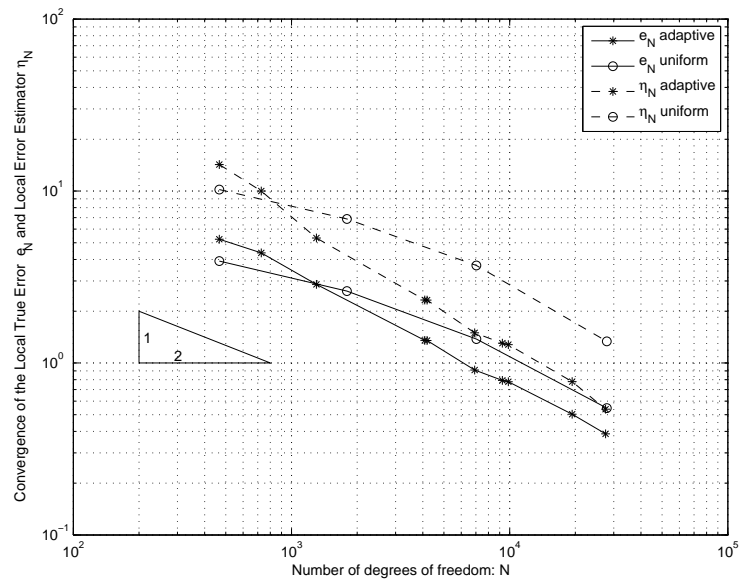


Figure 5.12: Semi-infinite plate: convergence of the local error and of the local error estimator, for uniform and adaptive refinements

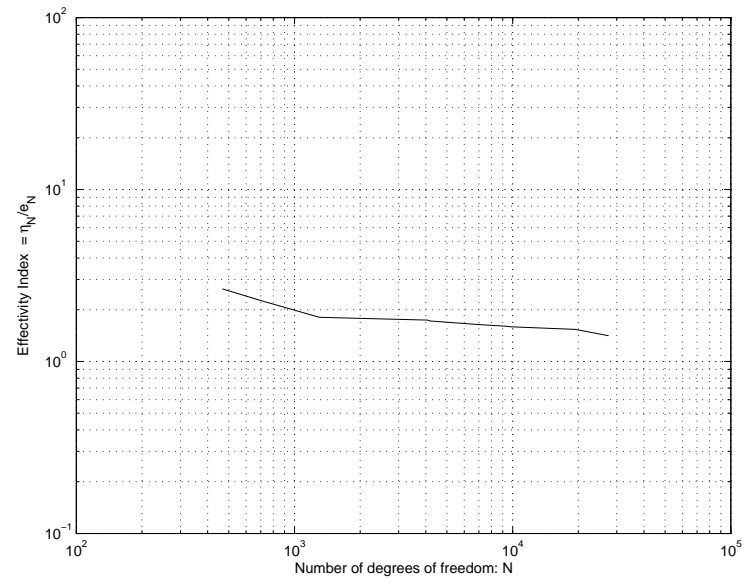
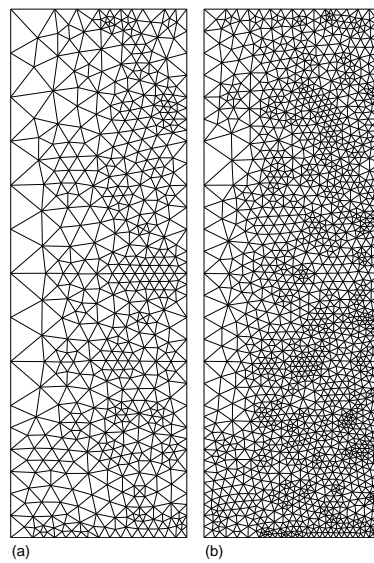


Figure 5.13: Semi-infinite plate: effectivity index for adaptive refinements

Figure 5.14: Semi-infinite plate: criss-cross mesh: seventh refinement step: $N=9262$, tenth refinement step: $N=27526$

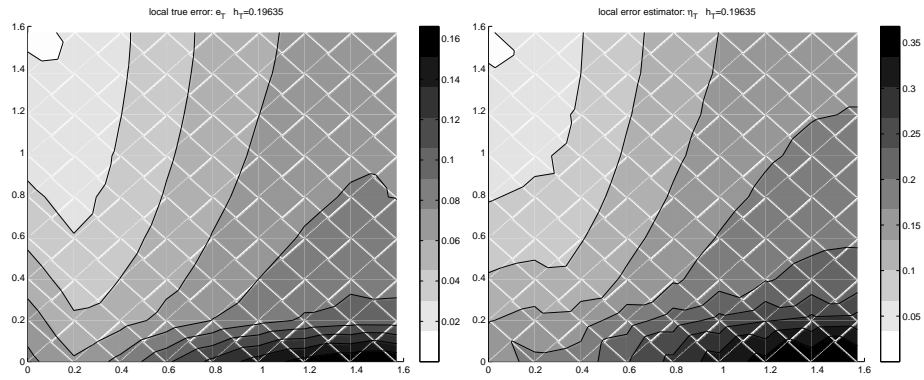


Figure 5.15: Semi-infinite plate, coarse mesh: local error and local residual distribution on a subdomain near the free boundary

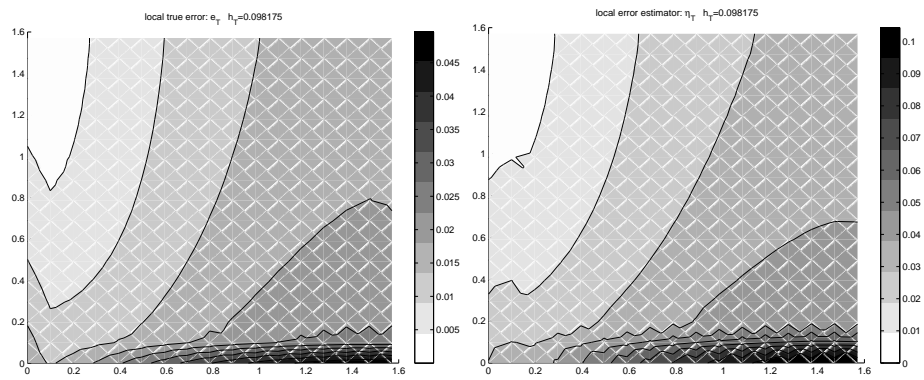


Figure 5.16: Semi-infinite plate, fine mesh: local error and local residual distribution on a subdomain near the free boundary